

## M Subdwarf Research III. Spectroscopic Diagnostics for Breaking Parameter Degeneracy

SHUO ZHANG (张硕) <sup>1,2</sup> HUA-WEI ZHANG (张华伟) <sup>1,2</sup> GEORGES COMTE,<sup>3</sup> DEREK HOMEIER <sup>4</sup> RUI WANG (王瑞) <sup>5</sup>  
NEDA HEJAZI <sup>6,7</sup> YIN-BI LI (李荫碧) <sup>5</sup> AND A-LI LUO (罗阿理) <sup>5,8</sup>

<sup>1</sup>Department of Astronomy, School of Physics, Peking University, Beijing 100871, P. R. China.

<sup>2</sup>Kavli institute of Astronomy and Astrophysics, Peking University, Beijing 100871, P. R. China.

<sup>3</sup>Aix-Marseille Univ, CNRS, CNES, LAM, Laboratoire d'Astrophysique de Marseille, Marseille, France.

<sup>4</sup>Zentrum für Astronomie der Universität Heidelberg, Landessternwarte, Knigstuhl 12, D-69117 Heidelberg, Germany

<sup>5</sup>CAS Key Laboratory of Optical Astronomy, National Astronomical Observatories, Beijing 100101, China

<sup>6</sup>Department of Physics and Astronomy, the University of Kansas, Lawrence, KS 66045, USA

<sup>7</sup>Department of Physics and Astronomy, Georgia State University, Atlanta, GA 30303, USA

<sup>8</sup>University of Chinese Academy of Sciences, Beijing 100049, China

### ABSTRACT

To understand the parameter degeneracy of M subdwarf spectra at low resolution, we assemble a large number of spectral features in the wavelength range 0.6-2.5  $\mu\text{m}$  with bandstrength quantified by narrowband indices. Based on the index trends of BT-Settl model sequences, we illustrate how the main atmospheric parameters ( $T_{\text{eff}}$ ,  $\log g$ ,  $[\text{M}/\text{H}]$  and  $[\alpha/\text{Fe}]$ ) affect each spectral feature differently. Furthermore, we propose a four-step process to determine the four parameters sequentially, which extends the basic idea proposed by Jao et al. Each step contains several spectral features that break the degeneracy effect when determining a specific stellar parameter. Finally, the feasibility of each spectroscopic diagnostic with different spectral quality is investigated. The result is resolution-independent down to  $R \sim 200$ .

*Keywords:* Stellar astronomy — Stellar types — Late-type stars — M stars

### 1. INTRODUCTION

Low-mass stars ( $M < 0.8M_{\odot}$ ) are the main stellar component of the Milky Way. They account for 70% of the number of stars and occupy 40% of the total stellar mass of the Galaxy (Reid & Gizis 1997; Chabrier 2003; Henry et al. 2006; Bochanski et al. 2010; Winters et al. 2015; Reylé et al. 2021). The M-type low-mass stars at the end of the main sequence in the H-R diagram contain a variety of exciting stellar components, including the most dominant stellar members of Galactic disk - M dwarfs, the rare Population II stars - M subdwarfs, and some of the substellar objects - degenerate brown dwarfs. M dwarfs have contributed significantly to studies of the initial mass function (e.g. Conroy & van Dokkum 2012; McConnell et al. 2016) as well as the mass-to-light ratio of nearby galaxies (Muirhead et al. 2015; Spiniello et al. 2015), and they are also popular

candidate hosts with earth-sized planet orbiting within the habitable zone (e.g., Dressing & Charbonneau 2013). Their metal-poor counterparts, subdwarfs that associated kinematically with the thick disk and halo (e.g., Bochanski et al. 2013), are of importance as the probes of the old galactic populations. Besides, young brown dwarfs with mass just below the hydrogen-burning minimum mass are sometimes classified to spectral types M7-M9, mixed with the ultracool dwarfs/subdwarfs with mass  $\leq 0.1M_{\odot}$  (Dupuy & Liu 2017; Zhang 2019).

As the members of old Galactic populations: old disk, thick disk, halo, bulge (see e.g. Mould 1976a; Lépine et al. 2007; Bochanski et al. 2013; Kesseli et al. 2019), M subdwarfs are rare in the solar neighborhood and are on average much older than the M dwarfs with solar-metallicity. The surface chemical compositions of these unevolved main-sequence stars are not changed by various enrichment processes and remain the chemical footprint of the gas from which they formed (e.g. Hejazi et al. 2022). This makes them fossil record and golden

tracers of the earliest phases of the assembly of the Milky Way.

Measuring basic atmospheric parameters is challenging for M-type low-mass stars, because the spectra of these stars with cool atmosphere (2500-4000 K) are dominated by molecular absorption bands, hiding or blending with the atomic lines, which leaves no windows onto the continuum (Allard 1990; Rajpurohit et al. 2014; Passegger et al. 2016). For M dwarfs, stellar properties have been studied relative thoroughly and generally determined separately. For example, effective temperature ( $T_{\text{eff}}$ ) of M dwarfs can be derived from empirical  $T_{\text{eff}}$ -color relationship (e.g., Mann et al. 2015, 2019) or  $T_{\text{eff}}$ -index relationship (Rojas-Ayala et al. 2012), while metallicity ([Fe/H]) can be estimated via relations of NIR K-band magnitudes alongside optical photometry (Bonfils et al. 2005; Neves et al. 2012) and calibrated by binaries containing an FGK-type companion (e.g., Bonfils et al. 2005; Mann et al. 2013a; Rains et al. 2021). Interferometric diameters and dynamical masses have been utilized to calibrate mass and radius relations (e.g. Delfosse et al. 2000; Benedict et al. 2016). In some works, comparing synthetic spectra over broad spectral ranges (Rajpurohit et al. 2013; Gaidos & Mann 2014; Du et al. 2021) or a series of selected feature bands (Passegger et al. 2016, 2018) to determine several parameters at once is opted for.

However, for metal-poor subdwarfs, the situation is more complicated, because metallicity severely affects the energy distribution in low-mass stars (Delfosse et al. 2000). Due to the scarcity in the solar neighborhood, it is difficult to obtain enough binaries containing metal-poor FGK star companion that can cover the entire metal abundance range. The low intrinsic brightness of subdwarfs further makes it difficult to acquire adequate high-resolution spectra covering the extended parameter grid, resulting in a poor constraint to the theoretical models. The near 1-to-1 mass-radius relation for the low-mass dwarfs (Benedict et al. 2016) is no longer effective because metal-deficiency modifies the equilibrium configuration of atmosphere of subdwarfs, leading to smaller radii at the same temperature (Kesseli et al. 2019). In addition, it is hard to obtain high-quality spectra in the optical because their spectral energy distributions peak at 0.8-1  $\mu\text{m}$ , while the infrared spectra are seriously contaminated by telluric absorption. To date, comparing observed spectra with grids of synthetic spectra, using  $\chi^2$  minimization in multi-dimensional parameter space is still the preferred method (Rajpurohit et al. 2013, 2014, 2016; Lodieu et al. 2019; Zhang et al. 2021; Hejazi et al. 2020, 2022).

When estimating parameters through a synthetic fitting process, parameter degeneracy usually occurs as a problem, because the strength of molecular features is a function of both  $T_{\text{eff}}$  and metallicity (Rains et al. 2021). For the metal-poor objects, the enhancement of  $\alpha$ -element (Ne, Mg, Si, S, Ar, Ca, Ti) also impacts the spectral shape over a wide range of wavelength regions (Hejazi et al. 2022). According to Hejazi et al. (2022) who conducted a study on pairwise degeneracy of  $T_{\text{eff}}$ ,  $\log g$ , [M/H], and [ $\alpha$ /Fe], the effects on the spectrum from increasing metal abundance within a certain range can be counteracted by the effect of an increase in  $T_{\text{eff}}$ , an increase in surface gravity or a decrease in [ $\alpha$ /Fe]. Therefore, uncertainty is introduced in the fitting process, due to a series of synthetic spectra with similar spectral morphology but different parameter combinations.

In this work, we aim to conduct an extended exploration of spectral degeneracy for M subdwarfs in the optical and near-infrared when more than two parameters are involved. The paper is organized as follows. Section 2 explores parameter degeneracy at various feature bands via spectral indices of model sequences. To break degeneracy, a four-step process for sequentially estimating  $T_{\text{eff}}$ , [M/H], [ $\alpha$ /Fe] and  $\log g$  is proposed. Section 3 discusses the effect from different spectral quality and resolution. Finally, we summarize our study in section 4.

## 2. SPECTROSCOPIC DIAGNOSTICS DETERMINATION

In the optical and near-infrared spectra of low-mass stars, the most significant opacity sources are metal oxide species such as TiO and CO, hydrides such as SiH, CaH, FeH, CrH, hydroxides such as CaOH, and water vapor (Rajpurohit et al. 2013, 2016). The molecular absorption features are consist of thousands of individual lines, affecting both the detailed structure of the spectrum and the global structure of the atmosphere (Valenti et al. 1998), blending to overlapped absorption bands in the low-resolution spectra.

Narrowband indices were usually designed to estimate the strengths of individual spectral features, which measure the flux ratios between the feature bands and sidebands (“pseudo-continuum”). Utilizing narrowband indices with a detailed understanding of corresponding spectral features, one can design effective schemes in estimating parameters. For example, Mould (1976b) predicted that TiO absorption decreases in strength with decreasing [M/H] but the hydride bands are largely unaffected, this qualitative result was quantified by Gizis (1997), who used several indices (CaH1, CaH2, CaH3,

TiO5) to measure the strengths of CaH and TiO bands and developed the first subdwarf classification system. It is worth noting that then a parameter  $\zeta_{\text{TiO/CaH}}$  was introduced by Lépine et al. (2007) to quantify the weakening of the TiO band strength. Its relationships with  $[\text{Fe}/\text{H}]$  and  $[\text{M}/\text{H}] + [\alpha/\text{Fe}]$  were determined by Woolf et al. (2009) and Hejazi et al. (2020), respectively.

The precondition of breaking degeneracy is a detailed understanding of the complicated dependence of more spectral features on atmospheric parameters. In this section, we propose a solution to parameter measurement, following and extending the basic idea of Jao et al. (2008) who proposed a 3-step method to break the degeneracy. The parameter degeneracy effect is further and deeply explored based on multiple spectral indices. Note that the analysis of the index trend is based on the synthetic spectra and hence influenced by the incompleteness of models. Nevertheless, these trends can still play a theoretical guiding role.

### 2.1. PHOENIX BT-Settl Model Grid

In the present study, we have used the latest BT-Settl CIFIST stellar atmosphere models (Allard et al. 2012, 2013, 2014; Baraffe et al. 2015) that also used in Hejazi et al. (2020, 2022). Compared with the classical grids available from the CIFIST project<sup>1</sup>, this newly calculated model grid<sup>2</sup> also varies over a range of alpha-element enhancements,  $[\alpha/\text{Fe}]$ , as a subgrid. These atmosphere models are computed with the PHOENIX multi-purpose atmosphere code version 15.5 (Hauschildt et al. 1997; Allard et al. 2001), including specialized models for the coolest (below 3000 K) stellar and brown dwarf atmospheres using the Settl model of cloud formation as well as the radiation hydrodynamic simulations of M-L-T dwarfs atmospheres (Freytag et al. 2010, 2012).

Since the release of the BT-Settl model atmospheres, the pre-calculated synthetic spectra have been widely used in numerous spectroscopic analyses with observations and measure the atmospheric parameters (e.g. Rajpurohit et al. 2013, 2014, 2016, 2018a,b; Mann et al. 2013b, 2015; Zhang et al. 2017a,b; Veyette et al. 2017; Zhang 2019; Hejazi et al. 2020, 2022; Zhang et al. 2021; Dieterich et al. 2021). The results show that BT-Settl models are successful in reproducing the overall optical-NIR spectral profile of M and L subdwarfs, particularly at  $[\text{Fe}/\text{H}] \leq -1.0$  dex (Zhang et al. 2017b), and most

of the molecular and atomic features can be well fitted with the observations (Rajpurohit et al. 2014).

In this work, we use the synthetic spectra instead of observed spectra for the subsequent investigation, because the parameter space of the model grid is uniform and extended to metallicities as low as  $[\text{M}/\text{H}] = -3.0$  dex, required for our analysis. The variation of a spectrum solely caused by changing atmospheric parameters can be explored. The parameter space is shown in Table 1 and the pre-calculated synthetic spectra have been convolved down to  $R \sim 2000$  in the following analyses. At this resolution, the uncertainty introduced by the imperfection of the models can be referred to the quantitative results from Hejazi et al. (2020, 2022), in which the authors measured that the maximum discrepancies between observation and best-fit synthetic spectra are 5%-15% depending on the temperature range and wavebands.

**Table 1.** Parameter space of the model grid used in this work

Variable	Range	Step size
$T_{\text{eff}}$	2500 - 4000 K	100 K
$\log g$	4.5 - 5.5 dex	0.5 dex
$[\text{M}/\text{H}]$	-3.0 - +0.5 dex	0.5 dex
$[\alpha/\text{Fe}]$	-0.2 - 0.2 dex for $[\text{M}/\text{H}] \geq 0.0$ 0.0 - 0.4 dex for $[\text{M}/\text{H}] = -0.5$ 0.2 - 0.6 dex for $[\text{M}/\text{H}] \leq -1.0$	0.2 dex

### 2.2. Exploration of Temperature Indicators

To serve as a qualified temperature indicator, spectral feature with such characteristics is expected: varying regularly and monotonically with the temperature and almost independent of the effects from any other atmospheric parameter. In the following, we examine and discuss a class of indices with such properties—pseudo-continuum colors—in a great detail.

#### 2.2.1. Pseudo-continuum colors

In general, the overall optical-to-NIR spectrum is largely depressed by molecular opacity in stars as cool as M subdwarfs, resulting the true stellar continuum can not be identified. However, at a few wavelength points, the molecules are a little more transparent, and one can see deeper in the photosphere, forming a pseudo-continuum (Kirkpatrick et al. 1991; Martin et al. 1996). Therefore, “pseudo-continuum colors” have been defined

<sup>1</sup> <https://phoenix.ens-lyon.fr/Grids/BT-Settl/CIFIST2011/>

<sup>2</sup> These models have not yet been made publicly available by the team.

to estimate the slope of the pseudo-continuum wavelength regions (Hamilton & Stauffer 1993; Martin et al. 1996; Martín et al. 1999; Hawley et al. 2002; Lépine et al. 2003; Covey et al. 2007; Yi et al. 2014).

We have collected 16 such “colors” from the literature and examined the dependence of each of them on atmospheric parameters. The pseudo-continuum colors are defined as

$$\text{Color} = \frac{\text{Average Flux Density (Numerator)}}{\text{Average Flux Density (Denominator)}} \quad (1)$$

where Numerator and Denominator are spectral regions within the reference wavelengths listed in Table A1. The results show that some of these colors are almost insensitive to metallicity and surface gravity, which makes them strong competitors for the temperature calibrators of subdwarfs.

To measure the variable value range of each color at different temperatures as closely as possible to real conditions, we select the entire model grid from 2500-4000 K with all available gravity, metallicity, and alpha enhancement values listed in Table 1, and measure the pseudo-continuum colors for each of these synthetic spectra. We then group the synthetic spectra by temperature, calculate the mean and standard deviation of all colors associated with the spectra in each group, as compared in Figure 1.

From the colors shown in the main panel of Figure 1, we find three colors with a quite small dispersion for each temperature group, and show them in the inner subfigure of Figure 1. The trend of the commonly used spectral typing indicator, CaH2+CaH3 (Lépine et al. 2007), is also demonstrated in this subfigure for comparison. Due to the exclusive dependence of the three pseudo-continuum colors, PC4, PC5, and Color-H02, on the temperature when  $T_{\text{eff}} \geq 3000$  K, we choose them to be the temperature indicators.

### 2.2.2. Two additional pseudo-continuum colors

Considering that all three selected colors have a reference band beyond 9000 Å where the observed spectra are dominated by strong telluric absorptions, we have further explored alternatives at bluer wavelengths. For this purpose, we have defined five bands listed in Table 2 pertaining to pseudo-continuum points within 6000-9000 Å which are less depressed by molecular opacity. Computed from every two bands, a pseudo-continuum color can measure the slope of the pseudo-continuum within the corresponding wavelength ranges. The upper panel of Figure 2 shows these bands on a synthetic spectrum, as an example.

**Table 2.** Pseudo-continuum bands defined in this work.

Band	Name	$\lambda_{\text{begin}}(\text{Å})$	$\lambda_{\text{end}}(\text{Å})$
1	C66	6590	6645
2	C70	7042	7049
3	C75	7545	7580
4	C81	8145	8165
5	C88	8833	8855

NOTE—The colors are named “CYY-XX” where YY and XX each represent a reference band and calculated following Equation 1, e.g., C81-66 =  $\frac{\text{Average Flux within Band 4}}{\text{Average Flux within Band 1}}$ .

After the exploration of all possible colors formed by the above five bands, we find that the pseudo-continuum slopes between the last three bands are mainly dependent on temperature, rather than other parameters. The dispersion of the pseudo-colors C88-81 and C81-75 are shown in the bottom panels of Figure 2. C88-81 has a regular dependence on the temperature, with a small and constant dispersion down to  $\sim 3000$  K. Note that the relatively small color range makes it a temperature indicator that would be subject to measurement uncertainties. On the other hand, C81-75 has a larger dynamic range, although its increasing dispersion towards lower temperatures may limit its applicability.

Caution should be taken when using these colors at low temperatures ( $T_{\text{eff}} < 3000$  K), where the color ranges related to the temperature groups rapidly increase. As temperature decreases below 3000 K, the increasing effect of molecular opacity and cloud formation on stellar atmospheres makes the modeling more complex and difficult (Allard et al. 2012). The optical spectra no longer change sensitively with  $T_{\text{eff}}$  due to dust formation (Rajpurohit et al. 2013). In addition, the pseudo-continuum colors also begin to be sensitive to other parameters. If they are still being used as temperature indicators, much larger uncertainty would thus be introduced.

In the following, we conduct a more extensive investigation of near-infrared spectral features redder than 1  $\mu\text{m}$  as a supplement and recommend some of them as temperature tracers for the ultracool subdwarfs.

### 2.2.3. Near-infrared temperature indicators

Spectroscopy at near-infrared wavelengths is involved with a wide range of available atomic and molecular

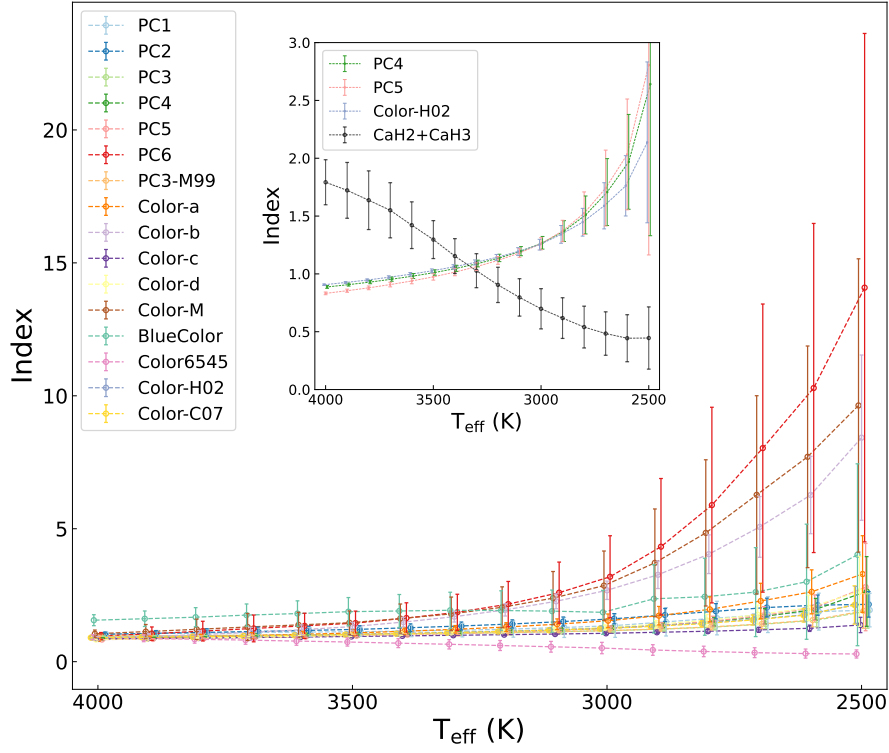


**Figure 1.** Main panel: the value dispersion of 16 psuedo-continuum colors defined in the literature. The entire model grid from 2500-4000 K with all available gravity, metallicity, and alpha enhancement values are used to calculate. The synthetic spectra are grouped by temperature, and the mean and standard deviation (shown as the error bar) of each group are calculated for each color. Inner panel: The three selected pseudo-continuum colors are shown comparing with the composite index CaH2+CaH3. Their typical dispersion values for different temperatures are listed in Table 3.

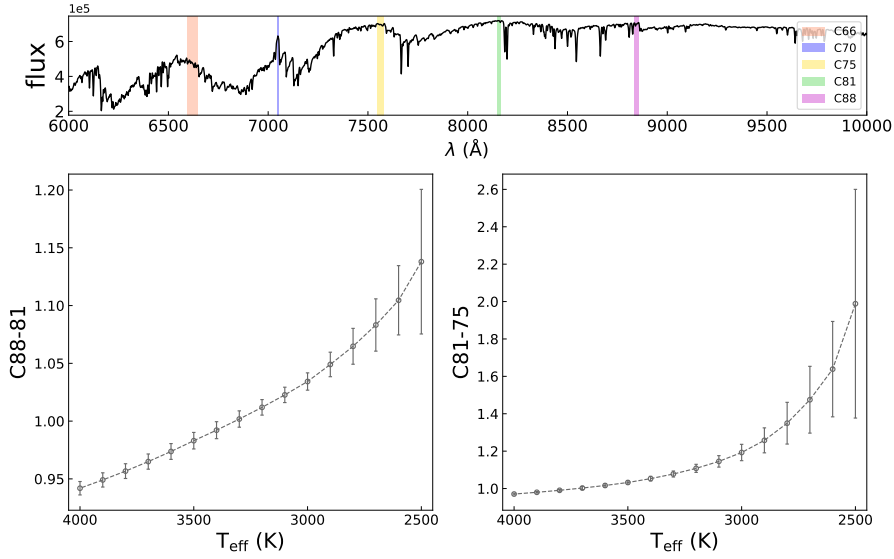


**Figure 2.** Upper panel: the bands listed in Table 2 shown on a synthetic spectrum of 3500 K. Bottom panels: two new pseudo-continuum colors defined in section 2.2.2 that are almost only sensitive to the effective temperature at  $T_{\text{eff}} \geq 3000$  K. Table 3 lists their typical dispersion values for different temperatures.

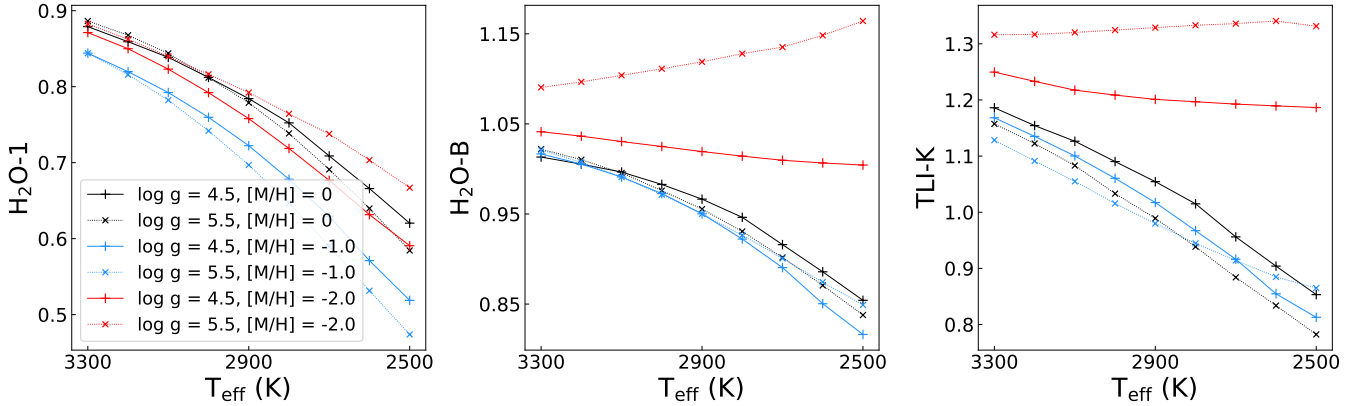
absorption features, especially water vapor absorption bands. Various studies on late-type M dwarfs and brown

dwarfs have defined spectral indices to characterize the

**Table 3.** Typical dispersion for different effective temperatures

Index	$T_{\text{eff}}$ (K)															
	4000	3900	3800	3700	3600	3500	3400	3300	3200	3100	3000	2900	2800	2700	2600	2500
CaH2+CaH3	0.1947	0.2412	0.2536	0.2383	0.2019	0.1640	0.1507	0.1470	0.1524	0.1618	0.1739	0.1759	0.1806	0.1878	0.2033	0.2690
PC4	0.0120	0.0125	0.0142	0.0181	0.0215	0.0233	0.0265	0.0291	0.0320	0.0394	0.0547	0.0901	0.1641	0.2892	0.4100	1.3107
PC5	0.0117	0.0135	0.0162	0.0199	0.0242	0.0282	0.0313	0.0327	0.0334	0.0373	0.0522	0.0924	0.1840	0.3280	0.4790	1.6421
Color-H02	0.0066	0.0079	0.0099	0.0129	0.0151	0.0168	0.0194	0.0219	0.0255	0.0334	0.0462	0.0767	0.1199	0.1996	0.2608	0.6954
C81-75	0.0047	0.0042	0.0050	0.0082	0.0091	0.0091	0.0121	0.0160	0.0216	0.0306	0.0437	0.0668	0.1116	0.1786	0.2551	0.6115
C88-81	0.0058	0.0062	0.0064	0.0066	0.0068	0.0072	0.0073	0.0071	0.0067	0.0067	0.0075	0.0106	0.0155	0.0226	0.0300	0.0626

NOTE—The typical dispersion values for the 5 pseudo-continuum colors at different effective temperatures. The classical compound index CaH2+CaH3 is presented for comparison.

**Figure 3.** Infrared indices as temperature indicators for ultracool subdwarfs. Models are plotted with the following codes: black refers to solar metallicity with  $[\alpha/\text{Fe}] = 0.0$ , blue refers to metallicity of  $-1.0$  dex with  $[\alpha/\text{Fe}] = 0.4$  dex, and red refers to  $-2.0$  dex with  $0.4$  dex; continuous lines for  $\log g = 4.5$  models and dotted lines for  $\log g = 5.5$  models.

molecular bands at different wavelengths, such as  $\text{H}_2\text{O}$ ,  $\text{CH}_4$ ,  $\text{CO}$ , and  $\text{FeH}$ .

We inspect the following 75 indices from the literature characterizing featurebands redder than  $1 \mu\text{m}$ : K1, K2 (Tokunaga & Kobayashi 1999), Q (Cushing et al. 2000), water index (McLean et al. 2000),  $\text{H}_2\text{O}^A$ ,  $\text{H}_2\text{O}^B$ ,  $\text{H}_2\text{O}^C$ ,  $\text{H}_2\text{O}^D$  (Reid et al. 2001), sHJ, sKJ,  $\text{sH}_2\text{O}^J$ ,  $\text{sH}_2\text{O}^{\text{H}1}$ ,  $\text{sH}_2\text{O}^{\text{H}2}$ ,  $\text{sH}_2\text{O}^{\text{K}}$  (Testi et al. 2001),  $\text{H}_2\text{O}-A$ ,  $\text{H}_2\text{O}-B$ ,  $\text{H}_2\text{O}-C$ ,  $\text{CH}_4-A$ ,  $\text{CH}_4-B$ ,  $\text{CH}_4-C$ , H/J, K/J, K/H, CO, 2.11/2.07, K shape (Burgasser et al. 2002),  $1.0 \mu\text{m}$ ,  $\text{H}_2\text{O}-1.2$ ,  $\text{H}_2\text{O}-1.5$ ,  $\text{CH}_4-1.6$ ,  $\text{H}_2\text{O}-2.0$ ,  $\text{CH}_4-2.2$  (Geballe et al. 2002),  $\text{H}_2\text{O}A$ ,  $\text{H}_2\text{O}B$ ,  $\text{H}_2\text{O}C$ ,  $\text{H}_2\text{O}D$ ,  $\text{CH}_4A$ ,  $\text{CH}_4B$ , CO, J-FeH, z-FeH (McLean et al. 2003),  $\text{H}_2\text{O}-1$ ,  $\text{H}_2\text{O}-2$ , FeH (Slesnick et al. 2004), z-VO (Cushing et al. 2005),  $\text{H}_2\text{O}-J$ ,  $\text{H}_2\text{O}-H$ ,  $\text{H}_2\text{O}-K$ ,  $\text{CH}_4-J$ ,  $\text{CH}_4-H$ ,  $\text{CH}_4-K$ , K/J (Burgasser et al. 2006),  $\text{H}_2\text{O}$ , Na (Allers et al. 2007), WH, WK, QH, QK (Weights et al. 2009), H-dip (Burgasser et al. 2010),  $\text{H}_2\text{O}-H$ ,  $\text{H}_2\text{O}-K$  (Covey et al. 2010),  $\text{H}_2\text{O}-K2$  (Rojas-Ayala et al. 2012), HPI (Scholz et al. 2012)  $\text{FeH}_z$ ,  $\text{VO}_z$ ,  $\text{FeH}_J K I_J$ , H-cont (Allers & Liu 2013),  $W_0$ ,  $W_D$ ,  $W_1$ ,  $W_2$  (Zhang et al. 2018), TLI-J, TLI-K, TLI-g (Almendros-Abad et al. 2022).

After evaluating the dependence on atmospheric parameters of all indices, we recommend to use three of them as temperature indicators:  $\text{H}_2\text{O}-1$ ,  $\text{H}_2\text{O}-B$ , and TLI-K. The indices can be calculated as

$$R_{\text{ind}} = \frac{F_{\text{W}}}{F_{\text{cont}}} \quad (2)$$

where pseudo-continuum ( $F_{\text{cont}}$ ) region and the feature ( $F_{\text{W}}$ ) wavelength limits are listed in Table A2.

As shown in Figure 3, the index  $\text{H}_2\text{O}-1$  has a regular temperature dependence at 2500-3500 K. Note that it also has a modest metal abundance dependence which increases slightly with decreasing temperature. Therefore, two other indices, i.e.,  $\text{H}_2\text{O}-B$  and TLI-K, are supplemented because they present more reliable temperature indicators for solar-abundant to moderately-metal-poor stars (dM/sdM).

In total, 8 spectral features consisting of 5 pseudo-continuum colors (3 from the literature and 2 defined in this work) and 3 spectral indices (redder than  $1 \mu\text{m}$ ) are provided as qualified temperature indicators.

### 2.3. Spectral Features for Estimating $[M/H]$ and $[\alpha/\text{Fe}]$

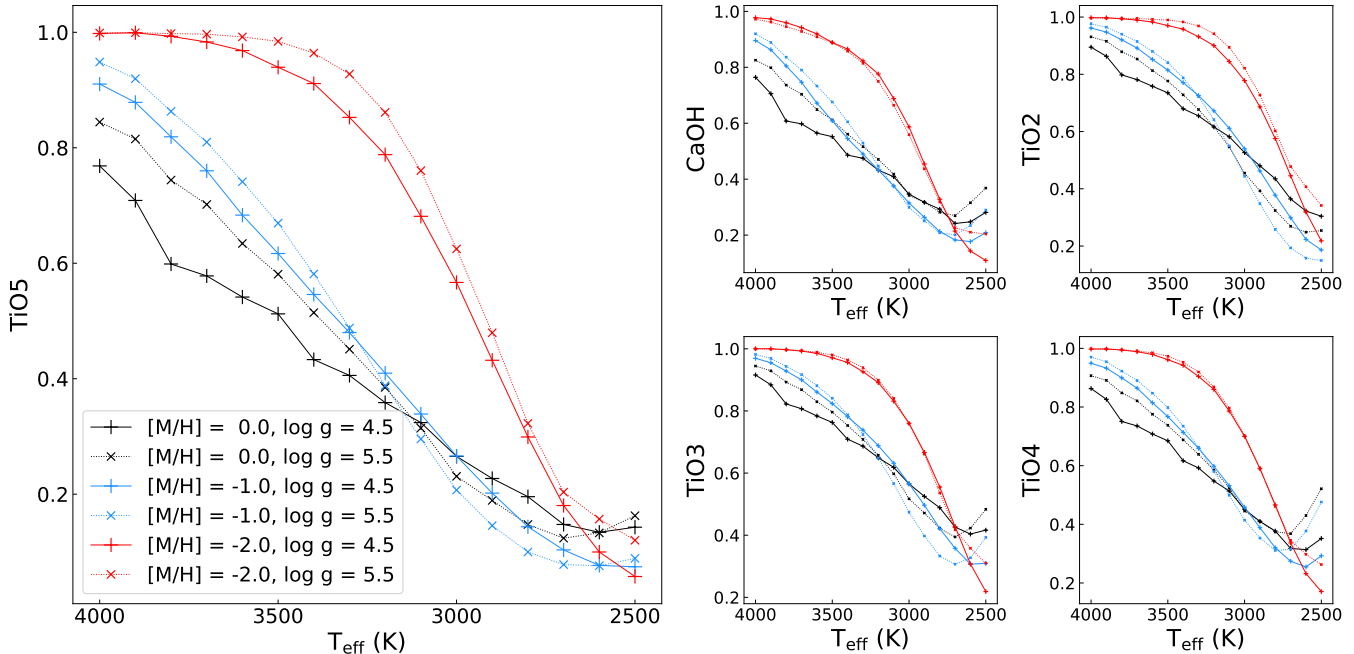


**Figure 4.** The TiO bands represented by the indices of TiO2, TiO3, TiO4 and TiO5 versus the effective temperature. In addition, the CaOH index behaving similarly with the TiO indices is also shown. Models are plotted with the same codes as in the above figure.

In the classification criteria of [Jao et al. \(2008\)](#), TiO5 band strength was used to determine metallicity level (see Section 5 in their paper) because the authors claimed that this band strength is highly sensitive to metal abundance variation while almost unaffected by surface gravity. In the left panel of Figure 4, we explore the complex dependence of TiO5 on atmospheric parameters based on model sequences with different metal abundances and surface gravity. Some other indices that have similar behavior, e.g., TiO2, TiO3, TiO4 and CaOH, are also shown in the right panels of Figure 4.

Two shortcomings limit the reliability of these indices as an indicator of metal abundance, as illustrated in Figure 4. First, at high temperatures ( $\sim 3300$ - $4000$  K), the index values for the solar metallicity to moderate metal-poor models are very sensitive to surface gravity. As shown in the left panel, increasing surface gravity and decreasing metal abundance have similar effects on TiO5 index values. Second, when the temperature drops below  $\sim 3300$  K, the index for the models of solar abundance to moderate metal deficiency ( $[M/H] = -1.0$  dex) loses its sensitivity to metal abundance, leaving the extremely metal-poor models as the only ones that can be distinguished. In addition, when the temperature drops below  $\sim 2700$  K, the index completely loses its ability to determine metal abundance levels due to the disappearance of the TiO molecular bands.

Besides, TiO is highly sensitive to  $\alpha$  abundance, which makes it an indicator of  $[\alpha/H]$  rather than the overall metallicity  $[M/H]$ . Although the values of  $[\alpha/Fe]$  and  $[M/H]$  generally maintain a correlation, the alpha abundances still differ for every single star and need to be determined individually. For example, the widely-used model grids such as the classical model grid from the CIFIST project or MARCS model grid ([Gustafsson et al. 2008](#)) assume  $[\alpha/Fe]$  as a function of  $[M/H]$  based on the rough estimate of  $[\alpha/Fe]$  for the thin and thick disk. For this reason,  $[\alpha/Fe]$  has been considered as a fixed parameter in many studies. However, large spectroscopic surveys like the Apache Point Observatory Galaxy Evolution Experiment (APOGEE; [Majewski et al. 2010](#); [Hayden et al. 2015](#)) and the Galactic Archaeology with HERMES (GALAH; [Buder et al. 2021](#)) have shown significant scatters around the tight relations assumed in the model grids.

The  $\alpha$  element abundance affects the spectral shape in roughly the same way with  $[M/H]$ . An increase in  $[M/H]$  may be counteracted by a decrease in  $[\alpha/Fe]$  and vice versa ([Hejazi et al. 2022](#)). Therefore, to infer more accurate  $[M/H]$ , one needs spectral features that are sensitive to neither surface gravity nor  $\alpha$  enhancement, but to changes in  $[M/H]$  from solar abundance to extreme metal deficiency (provided that the temperature has been already measured).

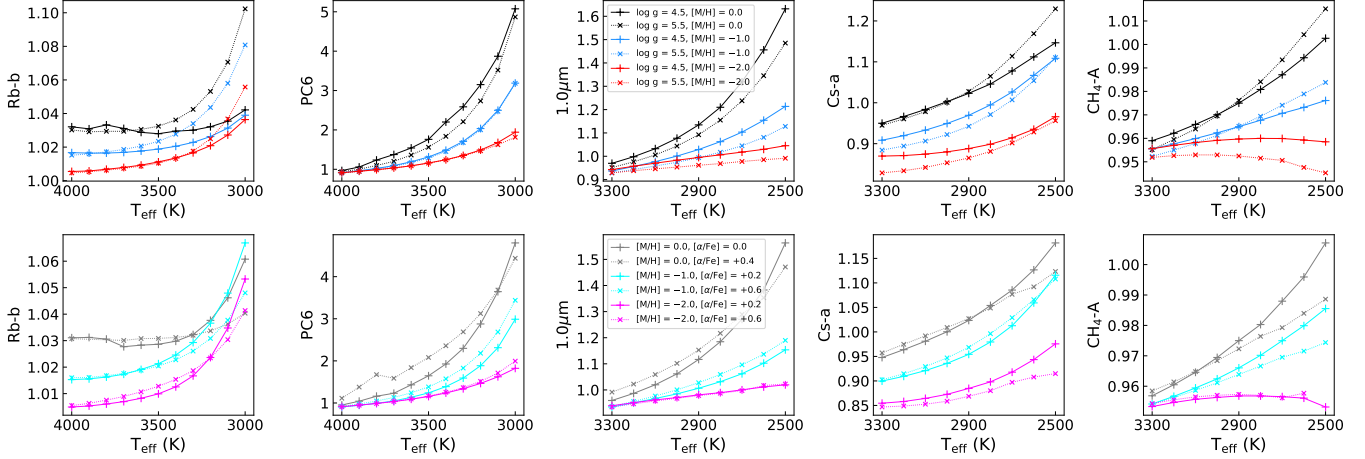


**Figure 5.** Spectral indices with low sensitivity to both surface gravity and alpha enhancement. The upper panels show the model sequences with the same color codes as in the figures above. The bottom panels show the same indices but of model sequences with  $\log g$  fixed at 5.0 and varied  $[\alpha/\text{Fe}]$  values.

To search for spectral features with such characteristics, we also explore more spectral features with reference wavebands within  $1 \mu\text{m}$  defined in the typical studies of M dwarfs/subdwarfs in addition to the NIR indices listed in Section 2.2.3, including CaH 6975, Ti I 7385, Na I 8183,8195 (Kirkpatrick et al. 1991), CaOH, CaH1, CaH2, CaH3, TiO1, TiO2, TiO3, TiO4, TiO5 (Reid et al. 1995), VO ratio (Kirkpatrick et al. 1995), TiO1, TiO2, VO1, VO2, CrH1, CrH2, FeH1, FeH2, H<sub>2</sub>O1 (Martín et al. 1999), VO-a, VO-b, Rb-b, Cs-a, CrH-a (Kirkpatrick et al. 1999), TiO 8440, VO 7434, VO 7912, Na 8190 (Hawley et al. 2002), TiO6, VO2 (Lépine et al. 2003), Ca I 4227, G band, Fe I 4383, Fe I 4405, Mg I 5172, Na D, Mg I 5172, TiO B, VO 7912, Na I 8189, Fe I 8689, Ca II 8498, Ca II 8542, Ca II 8662 (Covey et al. 2007), CaH, and TiO 8250 (Yi et al. 2014).

As a result, we select some of these indices for subsequent analysis and list their reference bands in Table A2. Five spectral indices exhibiting the expected characteristic within different temperature scopes are shown in Figure 5. In the temperature range of 3000-4000 K, Rb and PC6 show very little sensitivity to both gravity and alpha enrichment at high and low temperature end respectively. When the temperature drops to 3000 K and even lower, the indices  $1.0\mu\text{m}$ , Cs-a and CH<sub>4</sub>-A show the expected characteristics. These feature bands can be used to estimate  $[\text{M}/\text{H}]$  after the temperature is determined.

After  $[\text{M}/\text{H}]$  is determined, spectral features that are sensitive to  $[\alpha/\text{Fe}]$  but still independent of gravity can be used to estimate  $\alpha$  abundance. Here we provide three indicators, VO 7434, VO2, and Color-M99, as shown in Figure 6. VO 7434 exhibits good sensitivity to metal abundance at the high temperature end (3500-4000 K),

while VO2 and Color-M99 could well complement its lack of availability due to its increasing sensitivity to gravity at the low temperature end (2500-3500 K).

#### 2.4. Spectral Features for the Determination of Gravity

As a final step, spectral features that are highly sensitive to gravity are preferred to determine  $\log g$ . The classical CaH band strengths measured by indices CaH1, CaH2, and CaH3 are dependent on both metallicity and surface gravity. With the metal abundance determined as a precondition, they could be great indicators of gravity.

In addition to the CaH bands, hydrides such as FeH and the alkali lines such as Na I and K I doublet are all very sensitive to gravity. We recommend 4 indices shown in Figure 7, i.e., CaH1, Na 8190, FeH1 and Fe I 8689, because they have a high and regular sensitivity to gravity. Fe I 8689, Na 8190 present a strong gravity dependence for both solar abundance and moderately metal-poor model sequences. The index FeH1 has a significant dependence to the three parameters, which steadily becomes stronger towards lower temperatures. Most notably, the value of this index for the models with  $[\text{M}/\text{H}] = -2.0$  dex increases with decreasing temperature, while the index value for the solar-abundance and moderately metal-poor models decreases. Besides, models with high gravity are less sensitive to the temperature except for the extremely metal-poor ones.

#### 2.5. Parameter estimation steps

Accordingly, we can finally come up with a 4-step solution to the problem due to the degeneracy effect on the parameter determination of M subdwarfs.



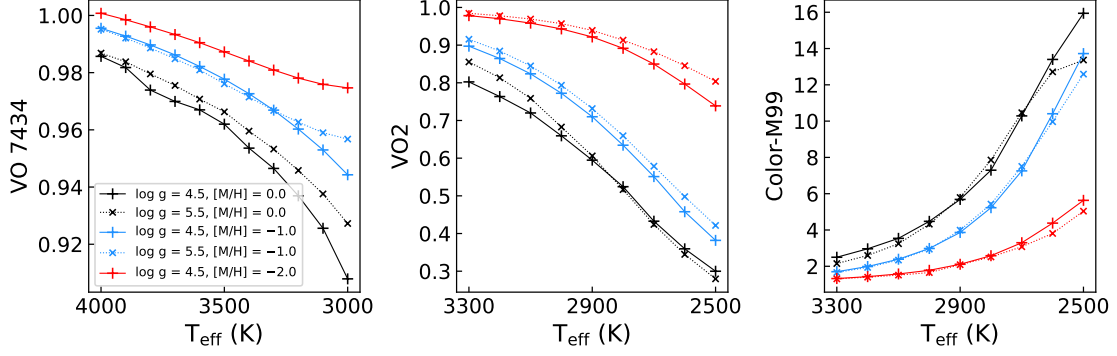


**Figure 6.** Models are plotted with the same color codes as in the above figures.

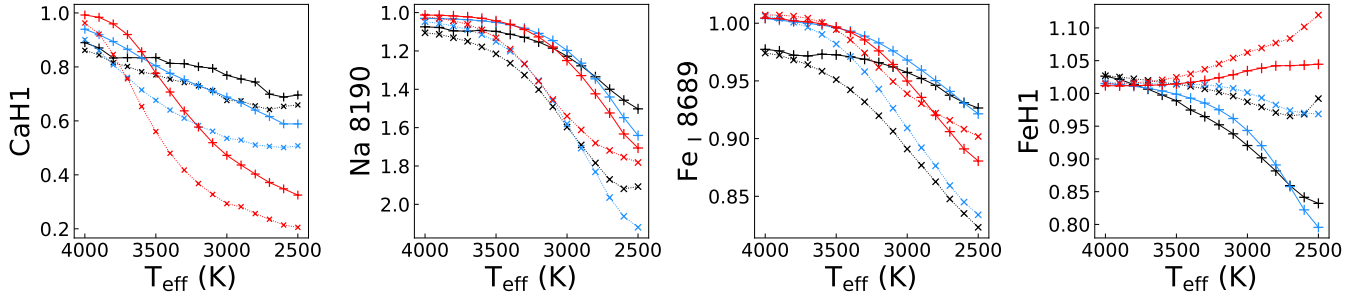


**Figure 7.** Indices that are highly sensitive to gravity and moderately sensitive to metallicity. Models are plotted with the same color codes as in the above figures.

1. The temperature-sensitive pseudo-continuum colors such as PC4, PC5, Color-H02, C88-81 and C81-75 can be used to estimate the temperature for a subdwarf, because these indices are hardly affected by the other atmospheric parameters. For the ultracool objects, infrared indices H<sub>2</sub>O-B, and TLI-K are recommended for the dMs and sdMs, while H<sub>2</sub>O-1 can be used for all the metallicity subclasses as temperature indicators with slightly larger scatters.
2. Based on the determined temperature, the spectral index/color Rb-b and PC6 can be used to estimate [M/H] for subdwarfs with temperatures higher than 3000 K because they are not sensitive to either  $[\alpha/\text{Fe}]$  or gravity within given temperature scope. For subdwarfs with temperatures lower than 3000 K, the indices 1.0  $\mu\text{m}$ , Cs-a and CH<sub>4</sub>-A could be useful.
3. The third free parameter, alpha enhancement  $[\alpha/\text{Fe}]$ , can be estimated from VO 7434, VO2 and Color-M99, as shown in Figure 6, when  $T_{\text{eff}}$  and [M/H] are known and fixed.
4. Finally, the spectral features that are particularly sensitive to surface gravity will be appropriate to

determine  $\log g$ . The multiple CaH bands (CaH1, CaH2, CaH3) are useful as good indicators, combining with the features measured by indices Na 8190, Fe I 8689 and FeH1.

Particular attention needs to be paid to the fact that each index has its own suitable temperature range and the results of these analyses are all based on low-resolution ( $R \sim 2000$ ) synthetic spectra.

Besides, considering that the dynamic range of each index is different, and the reference wavelength regions are also affected by observed factors differently, the applicable condition of each index is further discussed in the next section.

### 3. EFFECT FROM DIFFERENT SPECTRAL QUALITY AND RESOLUTION

The spectral indices were initially defined for low-resolution spectral research because low resolution spectra are readily available and plentiful but lack the detailed structures observed at high resolutions that can be used to accurately infer atmospheric parameters (see e.g. [Rajpurohit et al. 2014](#)).

In this section, we aim to investigate the effects from reduced spectral qualities which can be quantified by

signal-to-noise (S/N) ratios and lower spectral resolutions.

### 3.1. Spectral Quality Variations

All the model sequences in the  $T_{\text{eff}}$ -index diagrams above are based on the analysis results of the synthetic spectra without noise, but in the observations, the noise level of flux directly affects the measurement accuracy of the index. Therefore, we add Gaussian noises corresponding to S/N = 200, 100, 50, 20, 10, and 5 respectively to the synthetic spectra, calculate every index with the errors, and check the lowest S/N ratio that each index can still be used as a spectroscopic diagnostic.

As shown in Figure 8, in general, the pseudo-continuum colors are least affected by noise, and some (i.e., Color-H02, PC6, Color-M99) maintain some availability even when the S/N is as low as 5. On the contrary, a part of the diagnostics for metallicity and alpha abundance, i.e., Rb-b, Cs-a, CH<sub>4</sub>-A, VO-7434, depend very much on the quality of the spectrum: only when the S/N ratio exceeds 100, these indices distinguish finely between different abundances.

In addition, the effects that from observation and may introduce uncertainties need to be calibrated carefully in advance, such as telluric line contamination, flux calibration issues, spectral reddening and so on.

### 3.2. Lower Spectral Resolutions

At lower resolutions, problems could be raised by the information loss and the decreased number of sampling points involved in the index calculation.

As the resolution decreases, the overall shape of the SED remains basically unchanged, while the absorption lines become shallower and wider, the line-wings change from sharp to flat, and some more structural characteristics such as the “jagged” TiO molecular band near 7000 Å gradually smooths until almost invisible at R~200. Figure 9 shows a comparative example of a synthetic spectrum convolved to different resolutions.

On the other hand, the wavelength points within the reference bands of a spectral index decline in the number with the resolution decreasing. Assuming an observed spectrum is sampled with a proper sampling rate, e.g., 2.5 times the full width at half maximum (FWHM) of the line spread function (LSF), some very narrow reference bands may not have any points left to calculate when the resolution drops to R~500 or lower. In this situation, it is necessary to over-sample the observed spectrum before calculating any index.

In order to investigate the changes in the spectral indices caused by different resolutions and explore the applicability of these features, we additionally convolve the

synthetic spectra to R ~ 1000, 500, and 200, respectively.

The indices that are mostly influenced by the resolution variation are expected to be the absorption atomic lines (such as Na I doublet) and the narrow-band molecular features (such as TiO5 and CaH2/3) which has one narrow reference band as shown in the inner subfigure of Figure 9 - it is important to recall that the spectral features explored in this study have been measured by the average or integrated flux within several specific bands.

Nevertheless, upon closer inspection, we find that the vast majority of index trends of our recommended spectral features are resolution-independent down to R~200, while they are also affected by noise levels very similarly as at resolution R~2000. Since the performance of indices at these low resolutions is basically the same and does not provide significantly more information than Figure 8, we do not illustrate further the results here.

### 3.3. Discussion on Applicability to Observations

As a result, the exploration results of this paper can be also applied to very low-resolution spectral data, such as the slitless spectroscopic survey conducted by The Chinese Space Station Telescope (CSST; Zhan 2011, 2018; Gong et al. 2019) which aims to deliver high-quality spectra covering 2500-10,000 Å at R~200 for hundreds of millions of stars and galaxies. Even so, it is worth noting that flux calibration with high precision and high spectral quality are the foundation of the accuracy of index measurement. In many spectroscopic surveys, the flux calibration of cool stellar spectra often suffers larger uncertainty than the hot ones, mainly due to the lack of standard stars and inaccurate extinction correction.

We want to mention that, the above-proposed technique to solve the long-standing issue due to the parameter degeneracy is still in its early stage and more careful examinations are needed. In practice, a preset of initial values for the four parameters is required to start the a fitting process. We suggest using the approach presented in Hejazi et al. (2022) (Section 4.2 in their paper) which can allow us to develop an automated pipeline that will be applicable to future spectroscopic surveys.

In addition, a well-designed narrow-band photometric survey covering the selected wavelength bands can also be a competitive implementation option. In recent years, many narrow-band photometric surveys have been successfully carried out, such as the Javalambre Physics of the Accelerating Universe Astrophysical Survey (J-PAS; Marín-Franch et al. 2012; Benitez et al. 2014), the Javalambre-Photometric Local Universe Survey (J-PLUS; Cenarro et al. 2019; Yang et al. 2022; Wang et al. 2022), and the Southern Photometric Lo-

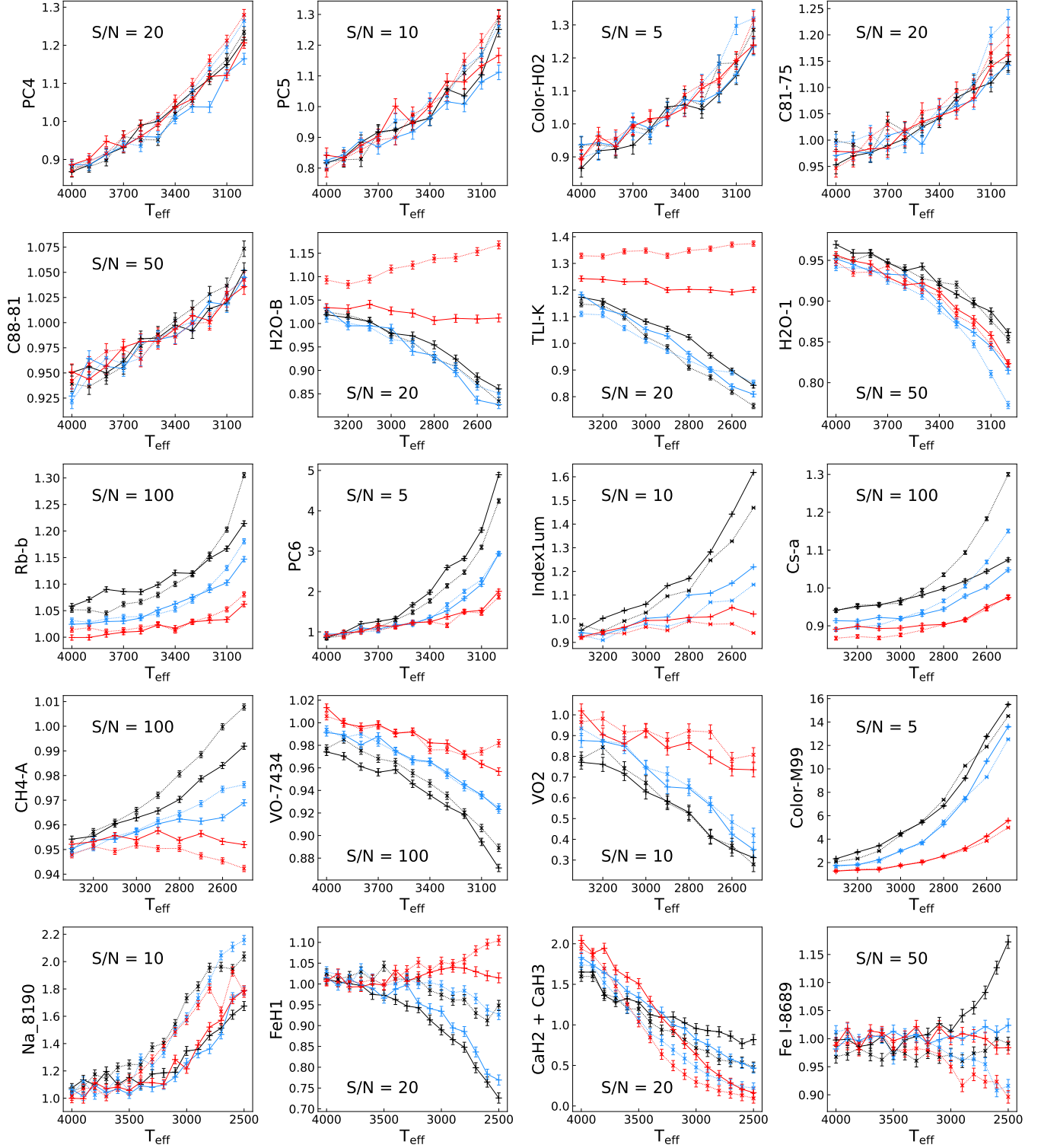


**Figure 8.** Recommended spectral indices derived from spectra with applicable lowest S/N ratios. The models are plotted with the same color codes as in the above figures. The error bars of each index representing  $1\sigma$  errors are calculated from synthetic spectra with Gaussian noise added. The corresponding S/N ratio is shown on each sub-diagram.

cal Universe Survey (S-PLUS; Mendes de Oliveira et al. 2019; Almeida-Fernandes et al. 2022). Color-H02 (7350-

7500 Å and 8900-9100 Å), for example, can be completely covered by filters 38 and 54 of J-PAS which used

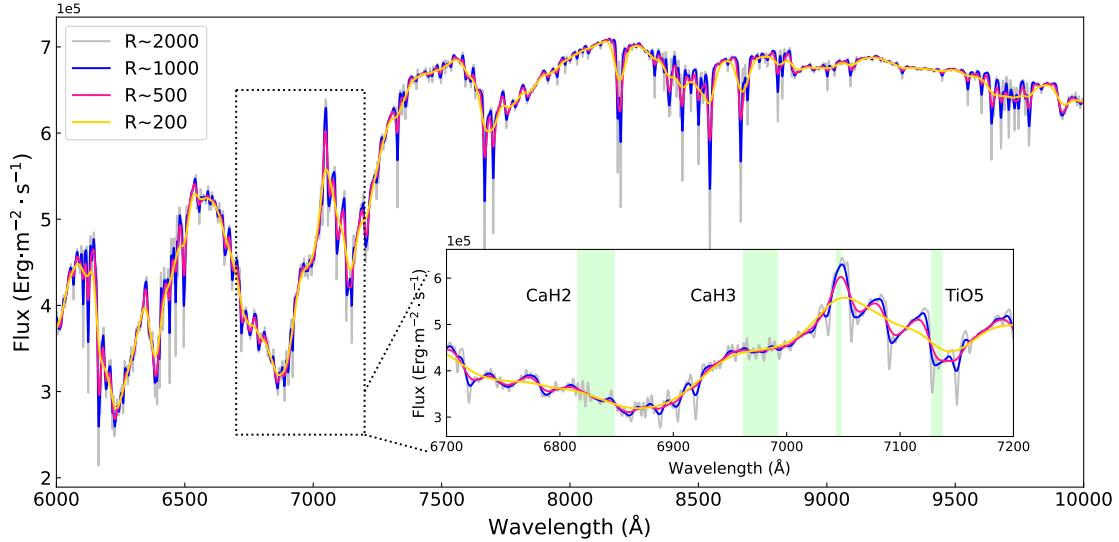


**Figure 9.** A synthetic spectrum ( $T_{\text{eff}} = 3500$  K,  $\log g = 5.0$ ,  $[M/H] = -1.0$  dex,  $[\alpha/Fe] = 0.4$  dex) at different resolutions: R~2000, 1000, 500, 200, respectively. The spectral region 6700-7200 Å is enlarged and shown in the inner subfigure. The CaH2, CaH3 and TiO5 feature bands and the reference band that they share are marked with lightgreen shadow.

56 narrow-band filters to sample the spectral energy distribution in the optical (3800-9200 Å) and achieved 1% photometric precision.

#### 4. SUMMARY AND CONCLUSION

In this paper, we conduct an extended exploration of parameter degeneracy of basic atmospheric parameters ( $T_{\text{eff}}$ ,  $\log g$ ,  $[M/H]$ , and  $[\alpha/Fe]$ ) in the optical to near-infrared spectra of M subdwarfs. We assemble a large number of pseudo-continuum colors and spectral indices which can quantify the slope of given pseudo-continuum and bandstrength of molecular absorption, respectively. Based on the index trends of the latest PHOENIX BT-Settl model sequences, we illustrate with figures how the degenerated parameters affect the bandstrength of each spectral feature.

Furthermore, we propose a four-step process (see Section 2.5) to determine  $T_{\text{eff}}$ ,  $[M/H]$ ,  $[\alpha/Fe]$  and  $\log g$  sequentially, which extends the basic idea proposed by Jao et al. and effectively breaks the degeneracy. To this end, we suggest several spectral features to be used in each step that determines a specific parameter. Note that although the suggested features are characterized by indices for our quantified investigation, the practical way to use these features may include, but not limited to,

selecting corresponding wavelength regions for spectral fitting, calculating index values and obtain empirical relationships, and adopting proper corresponding narrow-band photometry instead of spectral data.

The effect of different spectral quality and resolution are also explored, drawing a conclusion that pseudo-continuum colors are least affected by noise among the recommended spectral features, while some diagnostics for metallicity and alpha abundance depend very much on the quality of the spectrum. Most of index trends of spectral features that we recommended are resolution-independent down to R~200, but they are also affected by noise levels very similarly as at high resolution. Finally, we discuss the possibility of using narrow-band photometry as an alternative option for spectral data.

We thank the anonymous referee for helpful comments and suggestions which significantly improved our manuscript. Z.S. thanks Dr. Fu X.T. for the thoughtful discussion. This work was funded by the National Key R&D Program of China (No. 2019YFA0405500), the National Natural Science Foundation of China (NSFC Grant No. 11973001, 12090040, 12090044, 12103068), and the Science Research Grants from the China Manned Space Project with No. CMS-CSST-2021-B05, CMS-CSST-2021-A08.

#### APPENDIX

**Table A1.** The pseudo-continuum colors.

Pseudo-continuum Color	Name in this paper	Numerator( $\text{\AA}$ )	Denominator( $\text{\AA}$ )	Source
BlueColor		6100-6300	4500-4700	Covey et al. (2007)
Color6545		6545-6549	7560-7564	Yi et al. (2014)
Color-M		8105-8155	6510-6560	Lépine et al. (2003)
Color-1	Color-H02	8900-9100	7350-7500	Hawley et al. (2002)
Color-1	Color-C07	8900-9100	7350-7550	Covey et al. (2007)
Color-a		9800-9850	7300-7350	Kirkpatrick et al. (1999)
Color-b		9800-9850	7000-7050	Kirkpatrick et al. (1999)
Color-c		9800-9850	8100-8150	Kirkpatrick et al. (1999)
Color-d		9675-9875	7350-7550	Kirkpatrick et al. (1999)
PC1		7030-7050	6525-6550	Martin et al. (1996)
PC2		7540-7580	7030-7050	Martin et al. (1996)
PC3		8235-8265	7540-7580	Martin et al. (1996)
PC3	PC3-M99	8230-8270	7540-7580	Martin et al. (1999)
PC4		9190-9225	7540-7580	Martin et al. (1996)
PC5		9800-9880	7540-7580	Martin et al. (1996)
PC6		9090-9130	6500-6540	Martin et al. (1999)

NOTE—The pseudo-continuum colors assembled from the literature. Some of the colors are renamed to avoid the problem of duplicate names.

## A. PSEUDO-CONTINUUM COLORS AND SPECTRAL INDICES WITH THEIR REFERENCE BANDS

**Table A2.** The spectral features defined in the literature.

Spectral Index	Name in this paper	Numerator( $\text{\AA}$ )	Denominator( $\text{\AA}$ )	Method	Source
CaOH		6230-6240	6345-6354	average	Reid et al. (1995)
CaH1		6380-6390	6345-6355, 6410-6420	average	Reid et al. (1995)
CaH2		6814-6846	7042-7046	average	Reid et al. (1995)
CaH3		6960-6990	7042-7046	average	Reid et al. (1995)
TiO2		7058-7061	7043-7046	average	Reid et al. (1995)
TiO3		7092-7097	7079-7084	average	Reid et al. (1995)
TiO4		7130-7135	7115-7120	average	Reid et al. (1995)
TiO5		7126-7135	7042-7046	average	Reid et al. (1995)
VO 7434		7430-7470	7550-7570	average	Hawley et al. (2002)
VO2		7920-7960	8130-8150	average	Lépine et al. (2003)
Rb-b		7922.6-7932.6, 7962.6-7972.6	7942.6-7952.6	average	Kirkpatrick et al. (1999)
Na 8190		8140-8165	8173-8210	average	Hawley et al. (2002)
Fe I 8689		8684-8694	8664-8674	average	Covey et al. (2007)
Cs-a		8496.1-8506.1, 8536.1-8546.1	8516.1-8526.1	average	Kirkpatrick et al. (1999)
FeH1		8560-8660	8685-8725	average	Martin et al. (1999)
1.0 $\mu\text{m}$		10,400-10,500	8750-8850	integrated	Geballe et al. (2002)
CH <sub>4</sub> -A		12,950-13,250	12,500 12,800	average	Burgasser et al. (2002)
H <sub>2</sub> O-1		13,350-13,450	12,950-13,050	average	Slesnick et al. (2004)
H <sub>2</sub> O-B		15,050-15,250	15,750-15,950	average	Burgasser et al. (2002)
TLI-K		19,700-19,900	22,200-22,400	average	Almendros-Abad et al. (2022)

NOTE—Spectral indices assembled from the literature and recommended in the 4-step process. For each index, one can use the corresponding “Method” to calculate the flux over the “Numerator” and “Denominator” wavelength ranges respectively and derive the index value according to Equation 2. In the case of CaH1, Rb-b and Cs-a, two bands in Numerator/Denominator column are both used as the feature/pseudo-continuum.

## REFERENCES

- Allard, F. 1990, PhD thesis, Centre de Recherche Astrophysique de Lyon
- Allard, F., Hauschildt, P. H., Alexander, D. R., Tamanai, A., & Schweitzer, A. 2001, *ApJ*, 556, 357, doi: [10.1086/321547](https://doi.org/10.1086/321547)
- Allard, F., Homeier, D., & Freytag, B. 2012, *Philosophical Transactions of the Royal Society of London Series A*, 370, 2765, doi: [10.1098/rsta.2011.0269](https://doi.org/10.1098/rsta.2011.0269)
- Allard, F., Homeier, D., & Freytag, B. 2014, in *Astronomical Society of India Conference Series*, Vol. 11, *Astronomical Society of India Conference Series*, 33–45
- Allard, F., Homeier, D., Freytag, B., Schaffnerberger, W., & Rajpurohit, A. S. 2013, *Memorie della Societa Astronomica Italiana Supplementi*, 24, 128. <https://arxiv.org/abs/1302.6559>
- Allers, K. N., & Liu, M. C. 2013, *ApJ*, 772, 79, doi: [10.1088/0004-637X/772/2/79](https://doi.org/10.1088/0004-637X/772/2/79)
- Allers, K. N., Jaffe, D. T., Luhman, K. L., et al. 2007, *ApJ*, 657, 511, doi: [10.1086/510845](https://doi.org/10.1086/510845)
- Almeida-Fernandes, F., SamPedro, L., Herpich, F. R., et al. 2022, *MNRAS*, 511, 4590, doi: [10.1093/mnras/stac284](https://doi.org/10.1093/mnras/stac284)
- Almendros-Abad, V., Mužić, K., Moitinho, A., Krone-Martins, A., & Kubiak, K. 2022, *A&A*, 657, A129, doi: [10.1051/0004-6361/202142050](https://doi.org/10.1051/0004-6361/202142050)
- Baraffe, I., Homeier, D., Allard, F., & Chabrier, G. 2015, *A&A*, 577, A42, doi: [10.1051/0004-6361/201425481](https://doi.org/10.1051/0004-6361/201425481)
- Benedict, G. F., Henry, T. J., Franz, O. G., et al. 2016, *AJ*, 152, 141, doi: [10.3847/0004-6256/152/5/141](https://doi.org/10.3847/0004-6256/152/5/141)
- Benitez, N., Dupke, R., Moles, M., et al. 2014, *arXiv e-prints*, arXiv:1403.5237. <https://arxiv.org/abs/1403.5237>
- Bochanski, J. J., Hawley, S. L., Covey, K. R., et al. 2010, *AJ*, 139, 2679, doi: [10.1088/0004-6256/139/6/2679](https://doi.org/10.1088/0004-6256/139/6/2679)
- Bochanski, J. J., Savcheva, A., West, A. A., & Hawley, S. L. 2013, *AJ*, 145, 40, doi: [10.1088/0004-6256/145/2/40](https://doi.org/10.1088/0004-6256/145/2/40)
- Bonfils, X., Delfosse, X., Udry, S., et al. 2005, *A&A*, 442, 635, doi: [10.1051/0004-6361:20053046](https://doi.org/10.1051/0004-6361:20053046)
- Buder, S., Sharma, S., Kos, J., et al. 2021, *MNRAS*, 506, 150, doi: [10.1093/mnras/stab1242](https://doi.org/10.1093/mnras/stab1242)
- Burgasser, A. J., Cruz, K. L., Cushing, M., et al. 2010, *ApJ*, 710, 1142, doi: [10.1088/0004-637X/710/2/1142](https://doi.org/10.1088/0004-637X/710/2/1142)
- Burgasser, A. J., Geballe, T. R., Leggett, S. K., Kirkpatrick, J. D., & Golimowski, D. A. 2006, *ApJ*, 637, 1067, doi: [10.1086/498563](https://doi.org/10.1086/498563)
- Burgasser, A. J., Kirkpatrick, J. D., Brown, M. E., et al. 2002, *ApJ*, 564, 421, doi: [10.1086/324033](https://doi.org/10.1086/324033)
- Cenarro, A. J., Moles, M., Cristóbal-Hornillos, D., et al. 2019, *A&A*, 622, A176, doi: [10.1051/0004-6361/201833036](https://doi.org/10.1051/0004-6361/201833036)
- Chabrier, G. 2003, *PASP*, 115, 763, doi: [10.1086/376392](https://doi.org/10.1086/376392)
- Conroy, C., & van Dokkum, P. 2012, *ApJ*, 747, 69, doi: [10.1088/0004-637X/747/1/69](https://doi.org/10.1088/0004-637X/747/1/69)
- Covey, K. R., Lada, C. J., Román-Zúñiga, C., et al. 2010, *ApJ*, 722, 971, doi: [10.1088/0004-637X/722/2/971](https://doi.org/10.1088/0004-637X/722/2/971)
- Covey, K. R., Ivezić, Ž., Schlegel, D., et al. 2007, *AJ*, 134, 2398, doi: [10.1086/522052](https://doi.org/10.1086/522052)
- Cushing, M. C., Rayner, J. T., & Vacca, W. D. 2005, *ApJ*, 623, 1115, doi: [10.1086/428040](https://doi.org/10.1086/428040)
- Cushing, M. C., Tokunaga, A. T., & Kobayashi, N. 2000, *AJ*, 119, 3019, doi: [10.1086/301384](https://doi.org/10.1086/301384)
- Delfosse, X., Forveille, T., Ségransan, D., et al. 2000, *A&A*, 364, 217. <https://arxiv.org/abs/astro-ph/0010586>
- Dieterich, S. B., Simler, A., Henry, T. J., & Jao, W.-C. 2021, *AJ*, 161, 172, doi: [10.3847/1538-3881/abd2c2](https://doi.org/10.3847/1538-3881/abd2c2)
- Dressing, C. D., & Charbonneau, D. 2013, *ApJ*, 767, 95, doi: [10.1088/0004-637X/767/1/95](https://doi.org/10.1088/0004-637X/767/1/95)
- Du, B., Luo, A. L., Zhang, S., et al. 2021, *Research in Astronomy and Astrophysics*, 21, 202, doi: [10.1088/1674-4527/21/8/202](https://doi.org/10.1088/1674-4527/21/8/202)
- Dupuy, T. J., & Liu, M. C. 2017, *ApJS*, 231, 15, doi: [10.3847/1538-4365/aa5e4c](https://doi.org/10.3847/1538-4365/aa5e4c)
- Freytag, B., Allard, F., Ludwig, H. G., Homeier, D., & Steffen, M. 2010, *A&A*, 513, A19, doi: [10.1051/0004-6361/200913354](https://doi.org/10.1051/0004-6361/200913354)
- Freytag, B., Steffen, M., Ludwig, H. G., et al. 2012, *Journal of Computational Physics*, 231, 919, doi: [10.1016/j.jcp.2011.09.026](https://doi.org/10.1016/j.jcp.2011.09.026)
- Gaidos, E., & Mann, A. W. 2014, *ApJ*, 791, 54, doi: [10.1088/0004-637X/791/1/54](https://doi.org/10.1088/0004-637X/791/1/54)
- Geballe, T. R., Knapp, G. R., Leggett, S. K., et al. 2002, *ApJ*, 564, 466, doi: [10.1086/324078](https://doi.org/10.1086/324078)
- Gizis, J. E. 1997, *AJ*, 113, 806, doi: [10.1086/118302](https://doi.org/10.1086/118302)
- Gong, Y., Liu, X., Cao, Y., et al. 2019, *ApJ*, 883, 203, doi: [10.3847/1538-4357/ab391e](https://doi.org/10.3847/1538-4357/ab391e)
- Gustafsson, B., Edvardsson, B., Eriksson, K., et al. 2008, *A&A*, 486, 951, doi: [10.1051/0004-6361:200809724](https://doi.org/10.1051/0004-6361:200809724)
- Hamilton, D., & Stauffer, J. R. 1993, *AJ*, 105, 1855, doi: [10.1086/116559](https://doi.org/10.1086/116559)
- Hauschildt, P. H., Baron, E., & Allard, F. 1997, *ApJ*, 483, 390, doi: [10.1086/304233](https://doi.org/10.1086/304233)
- Hawley, S. L., Covey, K. R., Knapp, G. R., et al. 2002, *AJ*, 123, 3409, doi: [10.1086/340697](https://doi.org/10.1086/340697)
- Hayden, M. R., Bovy, J., Holtzman, J. A., et al. 2015, *ApJ*, 808, 132, doi: [10.1088/0004-637X/808/2/132](https://doi.org/10.1088/0004-637X/808/2/132)
- Hejazi, N., Lépine, S., Homeier, D., Rich, R. M., & Shara, M. M. 2020, *AJ*, 159, 30, doi: [10.3847/1538-3881/ab563c](https://doi.org/10.3847/1538-3881/ab563c)
- Hejazi, N., Lépine, S., & Nordlander, T. 2022, *ApJ*, 927, 122, doi: [10.3847/1538-4357/ac4e16](https://doi.org/10.3847/1538-4357/ac4e16)

- Henry, T. J., Jao, W.-C., Subasavage, J. P., et al. 2006, *AJ*, 132, 2360, doi: [10.1086/508233](https://doi.org/10.1086/508233)
- Jao, W.-C., Henry, T. J., Beaulieu, T. D., & Subasavage, J. P. 2008, *AJ*, 136, 840, doi: [10.1088/0004-6256/136/2/840](https://doi.org/10.1088/0004-6256/136/2/840)
- Kesseli, A. Y., Kirkpatrick, J. D., Fajardo-Acosta, S. B., et al. 2019, *AJ*, 157, 63, doi: [10.3847/1538-3881/aae982](https://doi.org/10.3847/1538-3881/aae982)
- Kirkpatrick, J. D., Henry, T. J., & McCarthy, Donald W., J. 1991, *ApJS*, 77, 417, doi: [10.1086/191611](https://doi.org/10.1086/191611)
- Kirkpatrick, J. D., Henry, T. J., & Simons, D. A. 1995, *AJ*, 109, 797, doi: [10.1086/117323](https://doi.org/10.1086/117323)
- Kirkpatrick, J. D., Reid, I. N., Liebert, J., et al. 1999, *ApJ*, 519, 802, doi: [10.1086/307414](https://doi.org/10.1086/307414)
- Lépine, S., Rich, R. M., & Shara, M. M. 2003, *AJ*, 125, 1598, doi: [10.1086/345972](https://doi.org/10.1086/345972)
- . 2007, *ApJ*, 669, 1235, doi: [10.1086/521614](https://doi.org/10.1086/521614)
- Lodieu, N., Allard, F., Rodrigo, C., et al. 2019, *A&A*, 628, A61, doi: [10.1051/0004-6361/201935299](https://doi.org/10.1051/0004-6361/201935299)
- Majewski, S. R., Wilson, J. C., Hearty, F., Schiavon, R. R., & Skrutskie, M. F. 2010, in *Chemical Abundances in the Universe: Connecting First Stars to Planets*, ed. K. Cunha, M. Spite, & B. Barbuy, Vol. 265, 480–481, doi: [10.1017/S1743921310001298](https://doi.org/10.1017/S1743921310001298)
- Mann, A. W., Brewer, J. M., Gaidos, E., Lépine, S., & Hilton, E. J. 2013a, *AJ*, 145, 52, doi: [10.1088/0004-6256/145/2/52](https://doi.org/10.1088/0004-6256/145/2/52)
- Mann, A. W., Feiden, G. A., Gaidos, E., Boyajian, T., & von Braun, K. 2015, *ApJ*, 804, 64, doi: [10.1088/0004-637X/804/1/64](https://doi.org/10.1088/0004-637X/804/1/64)
- Mann, A. W., Gaidos, E., & Ansdell, M. 2013b, *ApJ*, 779, 188, doi: [10.1088/0004-637X/779/2/188](https://doi.org/10.1088/0004-637X/779/2/188)
- Mann, A. W., Dupuy, T., Kraus, A. L., et al. 2019, *ApJ*, 871, 63, doi: [10.3847/1538-4357/aaf3bc](https://doi.org/10.3847/1538-4357/aaf3bc)
- Marín-Franch, A., Chueca, S., Moles, M., et al. 2012, in *Society of Photo-Optical Instrumentation Engineers (SPIE) Conference Series*, Vol. 8450, *Modern Technologies in Space- and Ground-based Telescopes and Instrumentation II*, ed. R. Navarro, C. R. Cunningham, & E. Prieto, 84503S, doi: [10.1117/12.925430](https://doi.org/10.1117/12.925430)
- Martín, E. L., Delfosse, X., Basri, G., et al. 1999, *AJ*, 118, 2466, doi: [10.1086/301107](https://doi.org/10.1086/301107)
- Martin, E. L., Rebolo, R., & Zapatero-Osorio, M. R. 1996, *ApJ*, 469, 706, doi: [10.1086/177817](https://doi.org/10.1086/177817)
- McConnell, N. J., Lu, J. R., & Mann, A. W. 2016, *ApJ*, 821, 39, doi: [10.3847/0004-637X/821/1/39](https://doi.org/10.3847/0004-637X/821/1/39)
- McLean, I. S., McGovern, M. R., Burgasser, A. J., et al. 2003, *ApJ*, 596, 561, doi: [10.1086/377636](https://doi.org/10.1086/377636)
- McLean, I. S., Wilcox, M. K., Becklin, E. E., et al. 2000, *ApJL*, 533, L45, doi: [10.1086/312600](https://doi.org/10.1086/312600)
- Mendes de Oliveira, C., Ribeiro, T., Schoenell, W., et al. 2019, *MNRAS*, 489, 241, doi: [10.1093/mnras/stz1985](https://doi.org/10.1093/mnras/stz1985)
- Mould, J. R. 1976a, *ApJ*, 210, 402, doi: [10.1086/154843](https://doi.org/10.1086/154843)
- . 1976b, *A&A*, 48, 443
- Muirhead, P. S., Mann, A. W., Vanderburg, A., et al. 2015, *ApJ*, 801, 18, doi: [10.1088/0004-637X/801/1/18](https://doi.org/10.1088/0004-637X/801/1/18)
- Neves, V., Bonfils, X., Santos, N. C., et al. 2012, *A&A*, 538, A25, doi: [10.1051/0004-6361/201118115](https://doi.org/10.1051/0004-6361/201118115)
- Passegger, V. M., Wende-von Berg, S., & Reiners, A. 2016, *A&A*, 587, A19, doi: [10.1051/0004-6361/201322261](https://doi.org/10.1051/0004-6361/201322261)
- Passegger, V. M., Reiners, A., Jeffers, S. V., et al. 2018, *A&A*, 615, A6, doi: [10.1051/0004-6361/201732312](https://doi.org/10.1051/0004-6361/201732312)
- Rains, A. D., Žerjal, M., Ireland, M. J., et al. 2021, *MNRAS*, 504, 5788, doi: [10.1093/mnras/stab1167](https://doi.org/10.1093/mnras/stab1167)
- Rajpurohit, A. S., Allard, F., Rajpurohit, S., et al. 2018a, *A&A*, 620, A180, doi: [10.1051/0004-6361/201833500](https://doi.org/10.1051/0004-6361/201833500)
- Rajpurohit, A. S., Allard, F., Teixeira, G. D. C., et al. 2018b, *A&A*, 610, A19, doi: [10.1051/0004-6361/201731507](https://doi.org/10.1051/0004-6361/201731507)
- Rajpurohit, A. S., Reylé, C., Allard, F., et al. 2016, *A&A*, 596, A33, doi: [10.1051/0004-6361/201526776](https://doi.org/10.1051/0004-6361/201526776)
- . 2013, *A&A*, 556, A15, doi: [10.1051/0004-6361/201321346](https://doi.org/10.1051/0004-6361/201321346)
- . 2014, *A&A*, 564, A90, doi: [10.1051/0004-6361/201322881](https://doi.org/10.1051/0004-6361/201322881)
- Reid, I. N., Burgasser, A. J., Cruz, K. L., Kirkpatrick, J. D., & Gizis, J. E. 2001, *AJ*, 121, 1710, doi: [10.1086/319418](https://doi.org/10.1086/319418)
- Reid, I. N., & Gizis, J. E. 1997, *AJ*, 114, 1992, doi: [10.1086/118620](https://doi.org/10.1086/118620)
- Reid, I. N., Hawley, S. L., & Gizis, J. E. 1995, *AJ*, 110, 1838, doi: [10.1086/117655](https://doi.org/10.1086/117655)
- Reylé, C., Jardine, K., Fouqué, P., et al. 2021, *A&A*, 650, A201, doi: [10.1051/0004-6361/202140985](https://doi.org/10.1051/0004-6361/202140985)
- Rojas-Ayala, B., Covey, K. R., Muirhead, P. S., & Lloyd, J. P. 2012, *ApJ*, 748, 93, doi: [10.1088/0004-637X/748/2/93](https://doi.org/10.1088/0004-637X/748/2/93)
- Scholz, A., Muzic, K., Geers, V., et al. 2012, *ApJ*, 744, 6, doi: [10.1088/0004-637X/744/1/6](https://doi.org/10.1088/0004-637X/744/1/6)
- Slesnick, C. L., Hillenbrand, L. A., & Carpenter, J. M. 2004, *ApJ*, 610, 1045, doi: [10.1086/421898](https://doi.org/10.1086/421898)
- Spiniello, C., Barnabè, M., Koopmans, L. V. E., & Trager, S. C. 2015, *MNRAS*, 452, L21, doi: [10.1093/mnrasl/slv079](https://doi.org/10.1093/mnrasl/slv079)
- Testi, L., D’Antona, F., Ghinassi, F., et al. 2001, *ApJL*, 552, L147, doi: [10.1086/320348](https://doi.org/10.1086/320348)
- Tokunaga, A. T., & Kobayashi, N. 1999, *AJ*, 117, 1010, doi: [10.1086/300732](https://doi.org/10.1086/300732)
- Valenti, J. A., Piskunov, N., & Johns-Krull, C. M. 1998, *ApJ*, 498, 851, doi: [10.1086/305587](https://doi.org/10.1086/305587)

- Veyette, M. J., Muirhead, P. S., Mann, A. W., et al. 2017, *ApJ*, 851, 26, doi: [10.3847/1538-4357/aa96aa](https://doi.org/10.3847/1538-4357/aa96aa)
- Wang, C., Bai, Y., Yuan, H., et al. 2022, arXiv e-prints, arXiv:2205.02595. <https://arxiv.org/abs/2205.02595>
- Weights, D. J., Lucas, P. W., Roche, P. F., Pinfield, D. J., & Riddick, F. 2009, *MNRAS*, 392, 817, doi: [10.1111/j.1365-2966.2008.14096.x](https://doi.org/10.1111/j.1365-2966.2008.14096.x)
- Winters, J. G., Henry, T. J., Lurie, J. C., et al. 2015, *AJ*, 149, 5, doi: [10.1088/0004-6256/149/1/5](https://doi.org/10.1088/0004-6256/149/1/5)
- Woolf, V. M., Lépine, S., & Wallerstein, G. 2009, *PASP*, 121, 117, doi: [10.1086/597433](https://doi.org/10.1086/597433)
- Yang, L., Yuan, H., Xiang, M., et al. 2022, *A&A*, 659, A181, doi: [10.1051/0004-6361/202142724](https://doi.org/10.1051/0004-6361/202142724)
- Yi, Z., Luo, A., Song, Y., et al. 2014, *AJ*, 147, 33, doi: [10.1088/0004-6256/147/2/33](https://doi.org/10.1088/0004-6256/147/2/33)
- Zhan, H. 2011, *Scientia Sinica Physica, Mechanica & Astronomica*, 41, 1441, doi: [10.1360/132011-961](https://doi.org/10.1360/132011-961)
- Zhan, H. 2018, in 42nd COSPAR Scientific Assembly, Vol. 42, E1.16–4–18
- Zhang, S., Luo, A. L., Comte, G., et al. 2021, *ApJ*, 908, 131, doi: [10.3847/1538-4357/abcf5](https://doi.org/10.3847/1538-4357/abcf5)
- Zhang, Z. 2019, *MNRAS*, 489, 1423, doi: [10.1093/mnras/stz2196](https://doi.org/10.1093/mnras/stz2196)
- Zhang, Z., Liu, M. C., Best, W. M. J., et al. 2018, *ApJ*, 858, 41, doi: [10.3847/1538-4357/aab269](https://doi.org/10.3847/1538-4357/aab269)
- Zhang, Z. H., Homeier, D., Pinfield, D. J., et al. 2017a, *MNRAS*, 468, 261, doi: [10.1093/mnras/stx350](https://doi.org/10.1093/mnras/stx350)
- Zhang, Z. H., Pinfield, D. J., Gálvez-Ortiz, M. C., et al. 2017b, *MNRAS*, 464, 3040, doi: [10.1093/mnras/stw2438](https://doi.org/10.1093/mnras/stw2438)